

# Three-dimensional vortex structures in a rotating dipolar Bose-Einstein condensate

Ramavarmaraja Kishor Kumar,<sup>1</sup> Thangarasu Sriraman,<sup>2</sup> Henrique Fabrelli,<sup>1</sup> Paulsamy Muruganandam,<sup>2</sup> and Arnaldo Gammal<sup>1</sup>

<sup>1</sup>*Instituto de Física, Universidade de São Paulo, 05508-090 São Paulo, Brazil*

<sup>2</sup>*School of Physics, Bharathidasan University, Tiruchirappalli 620024, Tamilnadu, India*

We study the three-dimensional ground state vortex lattice structures of purely dipolar Bose-Einstein condensate (BEC). By using the mean-field model we obtain a stability diagram for the vortex states in purely dipolar BECs as a function of harmonic trap aspect ratio ( $\lambda$ ) and dipole-dipole interaction strength ( $D$ ) under rotation. Rotating the condensate within the unstable region leads to collapse, while in the stable region furnishes stable vortex lattices of dipolar BECs. We analyse stable vortex lattice structures by solving three-dimensional time dependent Gross-Pitaevskii equation in imaginary time. Further, the stability of vortex states is examined by evolution in real-time. We also investigate distribution of vortices in fully anisotropic trap by increasing eccentricity of the external trapping potential. Breaking up of the condensate in two parts has been observed with equally shared vortices on each when the trap is sufficiently weak and the rotation frequency is high.

PACS numbers: 03.75.Lm, 67.85.De

## I. INTRODUCTION

Vortices in Bose-Einstein condensates of alkali atoms were first created and observed in laboratory during 1999 [1]. Since then a numerous experimental and theoretical studies along this direction devoted to explore the underlying physics [2, 3]. For instance, these studies include bending of vortex lines in cigar shaped trap, array of orderly aligned lattices in quantum-Hall regime, Tkachenko oscillations in lowest Landau level and so on [4, 5]. The rotational properties of BECs of alkali atoms are reviewed in Refs [6, 7]. Several techniques such as rotating the magnetic trap, laser stirring, decay of soliton, imprinting vortices using topological phases, superimposing an oscillating excitation to the trapping potential, and applying artificial magnetic fields [2, 8, 9] were adopted in BEC experiments to nucleate the vortices.

Early experiments and theoretical studies on vortices in BEC have been mostly focused on alkali Bose gas with local and isotropic interaction. In particular, there are many numerical studies proposed in the literature to analyze the stationary state of rotating alkali BECs [10]. However, the experimental realization of Bose-Einstein condensation in chromium (<sup>52</sup>Cr) [11], dysprosium (<sup>164</sup>Dy) [12], followed by erbium (<sup>168</sup>Er) [13] has enlightened the new direction in understanding the properties of BEC in dipolar quantum gases. The recent work in this direction has revealed a promoting physics due to the peculiar competition between isotropic short-range contact interaction and anisotropic long-range dipole-dipole interaction (DDI). The most significant features of the dipolar BECs are the emergence of biconcave-shape structured ground states, dependence of the stability on the trap geometry, the roton-like dip in the dispersion relation for excitation waves, and the  $d$ -wave mode of the collapse [14–17]. The rotational properties of dipolar Bose gases have also been studied theoretically in mean-

field regime [18–23]. These studies revealed that the rotational properties of dipolar BECs are strongly influenced by the harmonic trap aspect ratio, dipole-dipole interaction strength, contact interaction (CI) strength and relative strengths between DDI and CI [22, 23]. Square and triangular vortex lattice structures have been predicted in dipolar BECs loaded in optical lattice potential [24]. The stability of dipolar BEC is strongly depends on the trap geometry and dipolar interaction strength. So far the regime for the stability has been analyzed only for the ground state of dipolar BECs without rotation [25, 26]. Most of the previous studies on vortices in dipolar BECs are based on two dimensional models only [18–22]. However, it will be more realistic to investigate the stationary vortex structures in full three-dimensions as they are readily comparable with experiments.

In this paper, we study the ground state vortex lattice structures of purely dipolar Bose-Einstein condensate by considering the full three dimensional Gross-Pitaevskii equation. In particular, we analyse the stability regime for vortex state in purely dipolar BECs with respect to both trap aspect ratio and dipole-dipole interaction strength. The stability of the vortices is confirmed by numerically evolving the vortex states with real-time propagation. We show stationary vortex lattice structures for different trap aspect ratios within the stable regime. Further, we study the collapse dynamics of biconcave shape structured condensate during rotation. We also calculate certain physical quantities such as chemical potential, rms radius and angular momentum of condensate as a function of rotation frequency. We calculate the number of vortices using Thomas-Fermi approximation and compare them with that obtained through numerical simulations. Finally, we notice the breaking in condensate when the rotating dipolar BEC is in fully anisotropic trap. Actually the condensate breaks into two equal parts and shares an equal number of vortices in each part.

The paper is organized as follows. In Sec. II we present

the mean-field equation to study a dipolar BEC in a rotating trapping potential. In Sec. III we show a stability diagram for stable ground as well as vortex states in purely dipolar BECs as a function of harmonic trap aspect ratio and dipole-dipole interaction strength. In Sec. IV we study the stationary vortex structures observed numerically as well Thomas-Fermi calculation on some physical parameters during rotation of the condensate. Then we investigate the spatial distribution of vortices in fully anisotropic trap in Sec. V. Finally, in Sec. VI we present a brief summary and conclusion.

## II. THE MEAN-FIELD GROSS-PITAEVSKII EQUATION IN ROTATING FRAME

The pattern of vortices in the ground state of BEC can be studied using mean field Gross-Pitaevskii (GP) equation [6, 27]. At ultra-low temperatures the properties of a dipolar Bose-Einstein condensate of  $N$  atoms, each of mass  $m$ , can be described by the mean-field GP equation in rotating frame with nonlocal nonlinearity of the form [18, 21]:

$$i\hbar \frac{\partial \phi(\mathbf{r}, t)}{\partial t} = \left[ -\frac{\hbar^2}{2m} \nabla^2 + V_{\text{trap}}(\mathbf{r}) + \frac{4\pi\hbar^2 a N}{m} |\phi(\mathbf{r}, t)|^2 - \Omega L_z + N \int U_{\text{dd}}(\mathbf{r} - \mathbf{r}') |\phi(\mathbf{r}', t)|^2 d\mathbf{r}' \right] \phi(\mathbf{r}, t), \quad (1)$$

where  $\int d\mathbf{r} |\phi(\mathbf{r}, t)|^2 = 1$ . The trapping potential,  $V_{\text{trap}}$  is assumed to be fully asymmetric of the form

$$V_{\text{trap}}(\mathbf{r}) = \frac{1}{2} m (\omega_x^2 x^2 + \omega_y^2 y^2 + \omega_z^2 z^2)$$

where  $\omega_x, \omega_y$  and  $\omega_z$  are the trap frequencies,  $a$  the atomic scattering length.  $L_z = -i\hbar(x\partial_y - y\partial_x)$  corresponds to the  $z$ -component of the angular momentum due to the rotation of the dipolar BEC about  $z$ -axis with rotation frequency  $\Omega$ .

The dipolar interaction, for magnetic dipoles, is given by [28, 29]

$$U_{\text{dd}}(\mathbf{R}) = \frac{\mu_0 \bar{\mu}^2}{4\pi} \frac{1 - 3\cos^2\theta}{|\mathbf{R}|^3} \left( \frac{3\cos^2\varphi - 1}{2} \right), \quad (2)$$

where  $\mathbf{R} = \mathbf{r} - \mathbf{r}'$  determines the relative position of dipoles and  $\theta$  is the angle between  $\mathbf{R}$  and the direction of polarization,  $\mu_0$  is the permeability of free space and  $\bar{\mu}$  is the dipole moment of the condensate atom. The  $\varphi$  is the angle between the orientation of dipoles and  $z$ -axis. We consider the polarization of magnetic dipoles along the direction of  $z$ -axis as long as  $\varphi = 0$ . Nevertheless it is tunable to change the dipolar interaction from attractive to repulsive.

To compare the contact and dipolar interactions, often it is convenient to introduce the length scale  $a_{\text{dd}} \equiv \mu_0 \bar{\mu}^2 m / (12\pi\hbar^2)$  [30]. The chromium has a magnetic

dipole moment of  $\bar{\mu} = 6\mu_B$  ( $\mu_B$  is the Bohr magneton) so that  $a_{\text{dd}} \simeq 16a_0$ , where  $a_0$  is the Bohr radius. The dipole-dipole interaction strength is expressed as  $D = 3Na_{\text{dd}}$ .

Convenient dimensionless parameters can be defined in terms of a reference frequency  $\bar{\omega}$  and the corresponding oscillator length  $l = \sqrt{\hbar/(m\bar{\omega})}$ . Using dimensionless variables  $\mathbf{r}' = \mathbf{r}/l, \mathbf{R}' = \mathbf{R}/l, a' = a/l, a'_{\text{dd}} = a_{\text{dd}}/l, t' = t\bar{\omega}, x' = x/l, y' = y/l, z' = z/l, \Omega' = \Omega/\bar{\omega}, \phi' = l^{3/2}\phi$ , Eq. (1) can be rewritten (after dropping the primes from all the variables) as

$$i \frac{\partial \phi(\mathbf{r}, t)}{\partial t} = \left[ -\frac{1}{2} \nabla^2 + \frac{1}{2} (\gamma^2 x^2 + \nu^2 y^2 + \lambda^2 z^2) + 4\pi a N |\phi|^2 - \Omega L_z + 3Na_{\text{dd}} \int V_{\text{dd}}^{3D}(\mathbf{R}) |\phi(\mathbf{r}', t)|^2 d\mathbf{r}' \right] \phi(\mathbf{r}, t), \quad (3)$$

with

$$V_{\text{dd}}^{3D}(\mathbf{R}) = \frac{1 - 3\cos^2\theta}{|\mathbf{R}|^3} \left( \frac{3\cos^2\varphi - 1}{2} \right), \quad (4)$$

$\gamma = \omega_x/\bar{\omega}, \nu = \omega_y/\bar{\omega}, \lambda = \omega_z/\bar{\omega}$ . We consider the cylindrically symmetric harmonic trap with  $\gamma = \nu$  with  $\omega_x = \omega_y = \omega_\rho$  and we use the reference frequency  $\bar{\omega}$  as  $\omega_\rho$ . For the fully anisotropic trap, the reference frequency is taken as the geometric mean, that is,  $\bar{\omega} = (\omega_x \omega_y \omega_z)^{1/3}$ . From now, we only refer to the dimensionless variables.

We perform numerical simulation of the 3D GP equation (3) using the split-step Crank-Nicolson method described in Ref. [31, 32]. The dipolar integral in Eq. (3) diverges at short distance in coordinate space, however this intricacy can be circumvent by evaluating the integral in momentum space [29, 33].

## III. GROUND STATE AND VORTEX STABILITY

The important feature of dipolar BEC is the emergence of unusual structured ground states in pancake trap. So far many theoretical studies has exposed to analyze the stability and ground state structures of dipolar BECs. The remarkable ground state which looks alike a biconcave shaped structure with maximum of density not in the center has recognized [25, 26]. Furthermore, the density oscillations of dipolar BEC with two and four peaks were also been reviewed in fully anisotropic trap. Along the way, we are interested to study the stability and ground state structures in purely dipolar BEC in pancake trap. We have composed the stability diagram for a purely dipolar BEC as a function of trap aspect ratio ( $\lambda$ ) and dipolar interaction strength ( $D$ ), a similar stability diagram given in Ref. [25]. A dipolar BEC is unstable and collapses for the number of atoms  $N$  above a critical value. This can be studied by solving the three-dimensional time-dependent GP equation (3).

We have broadened the stability diagram to  $\lambda = 30$  and calculated the stability region of ground state solutions. The biconcave shaped condensate density as

shown in Fig. 1 is obtained for the parameters ( $\lambda = 7$  and  $D = 30.4$ ). One may note that similar biconcave structures are shown in Refs. [25, 26]. Also, we observed

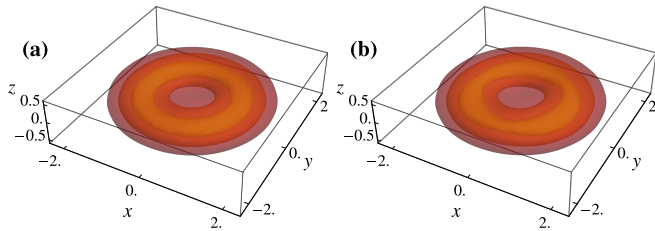


FIG. 1. (Color online) Three-dimensional contour plot showing the transparent view of density oscillation of biconcave shape structured condensate in the absence of rotation ( $\Omega = 0$ ) evolve in real-time at time, (a)  $t = 0$  and (b)  $t = 500$ . The contours levels are taken as  $|\phi|^2 = 0.03, 0.04$  and  $0.05$

such local density fluctuation for the following trap aspect ratios  $\lambda = 7, 8, 11, 12, 15, 16, 19$ , and  $20$ . The structured condensates are locally stable in the sense they are stable only with in local minimum of the energy. Further

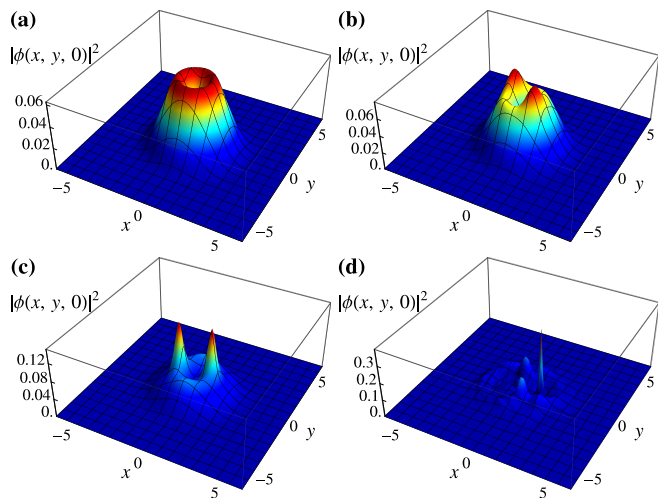


FIG. 2. (Color online) The condensate density  $|\phi(x, y, 0)|^2$  in  $xy$  plane showing the collapse dynamics of rotating biconcave shape structured condensate with  $\Omega = 0.5$  in real-time at time, (a)  $t = 0$ , (b)  $t = 60$ , (c)  $t = 64$ , and (d)  $t = 65$ .

increase in number of particles or increase in dipolar interaction energy will change the structured state to unstable. Here we are interested to rotate this biconcave shaped condensate to study the time evolution. With this objective, we prepared the ground state solution by solving the Eq. (3) using imaginary time propagation in the absence of rotation ( $\Omega = 0$ ) and then seed the resulting solution in realtime propagation by applying rotation with frequency  $\Omega = 0.5$ . At the time of rotation the dipoles are immensely pulled towards the outer rim and two peaks are formed as shown in Fig. 2 (b). This two peak is sustained for a very short time and biconcave

shaped condensate becomes unstable. The corresponding collapse dynamics during rotation is shown as two- and three-dimensional view in Figs. 2 and 3, respectively. Further, we have constructed a phase diagram illustrat-

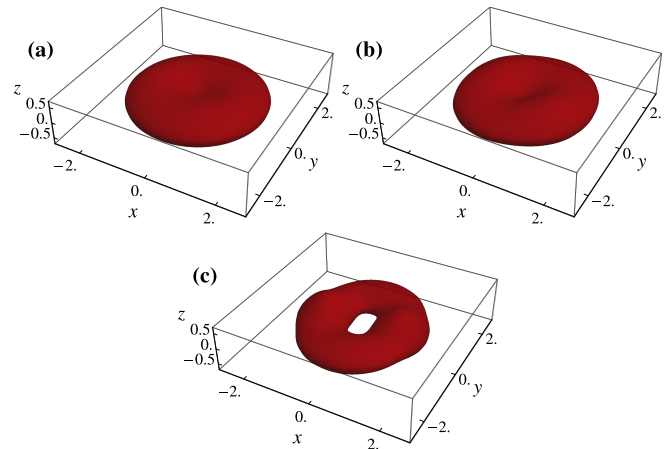


FIG. 3. (Color online) Three-dimensional contour plots of the density  $|\phi(x, y, z)|^2$  taken at 0.04 of the condensate showing the rotating biconcave shape structured condensate with  $\Omega = 0.5$  in real-time propagation at time. (a)  $t = 0$ , (b)  $t = 60$ , and (c)  $t = 64$ .

ing the stability region for stable vortices in  $\lambda-D$  parameter space as shown in Fig. 4. The stable region for vor-

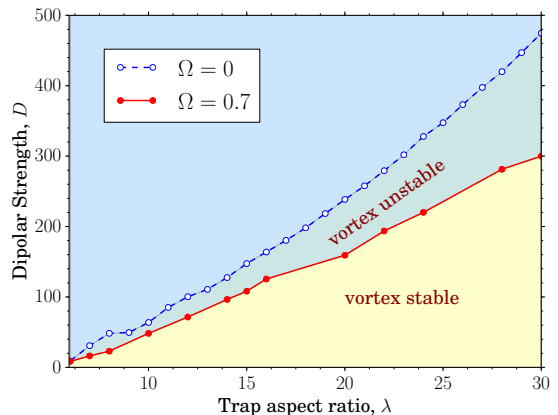


FIG. 4. (Color online) Stability diagram of a purely dipolar BEC in cylindrically symmetric trap as a function of trap aspect ratio ( $\lambda$ ) and dipolar interaction parameter ( $D$ ). Below the dotted blue line the ground state is stable while below the solid line is the region of stable vortices

tex state is located below the stability region of ground states (dashed blue line with empty circles) in Fig. 4. In order to carry out this observation, we have prepared the ground state solution using imaginary time propagation with ( $\Omega = 0$ ) and progress the solution in imaginary-time with rotation frequency  $\Omega = 0.7$ . Nevertheless the stability diagram has been checked for the rotation frequencies

in the range 0.7 and 0.99 and no significant changes in the stability boundary are observed. Also, we examined the stability of stationary vortex state solutions by evolving using real-time propagation. In Fig. 4, the region below the solid red line with filled circles there exist stable vortex states. While in the region between the dashed blue with empty circles and solid red line with filled circles the vortex states are not stable. In the next section, we shall discuss the feasible vortex structures in the shaded region below the solid red line. For the present study we mainly consider two different harmonic trap aspect ratios,  $\lambda = 10$  and 30, and the dipolar interaction strength is chosen within the vortex stable region in Fig. 4.

#### IV. STATIONARY VORTEX LATTICES IN PURELY DIPOLAR BECS

In the following, we show several stationary vortex structures in purely dipolar BEC in the different harmonic trap aspect ratios  $\lambda = 10$  and 30, and correspondingly the dipolar interaction strength is chosen as  $D \simeq 38$  and 300, respectively. First, in Fig. 5, we show the stationary vortex structures in  $\lambda = 10$ . We prepare the

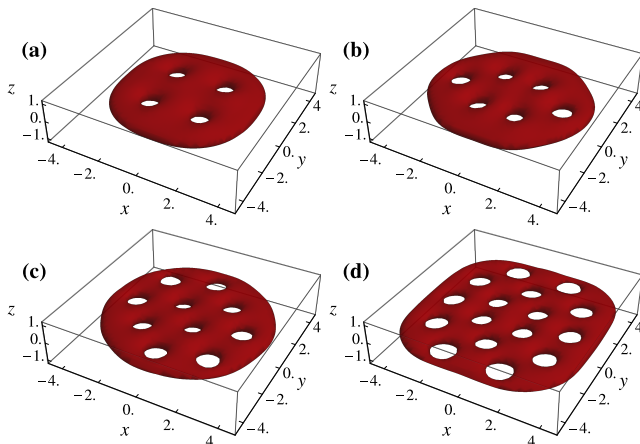


FIG. 5. (Color online) Three-dimensional view of condensate density  $|\phi(x, y, z)|^2$  at 0.0125 with vortex lattice of purely dipolar BECs with  $a_{dd} = 16 a_0$ ,  $a = 0$ ,  $D = 38$ ,  $\lambda = 10$ . at rotation frequencies (a)  $\Omega = 0.5$ , (b)  $\Omega = 0.7$ , (c)  $\Omega = 0.8$  and (d)  $\Omega = 0.97$ .

ground state wave function by solving Eq. (3) in the absence of rotation ( $\Omega = 0$ ). The vortices are then created by evolving the ground state with the inclusion of rotation ( $\Omega \neq 0$ ) to witness the stationary vortex structures. When the condensate begins to rotate the multiply quantized vortices enter into the condensate from the surface. As time progress these vortices approach to a stationary vortex configuration as shown in Fig. 5. We notice the hexagonal vortex structure at rotation frequency  $\Omega = 0.7$ . Usually centered single vortex surrounded by five vortices is the basic configuration. Whereas, here

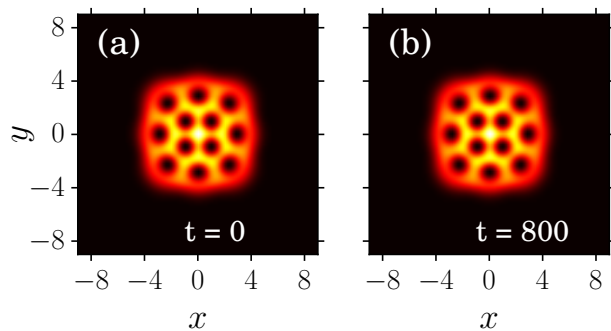


FIG. 6. (Color online) Two-dimensional view of the stable evolution of the condensate density  $|\phi(x, y, 0)|^2$  with vortices arranged in a square lattice with  $a_{dd} = 16 a_0$ ,  $a = 0$ ,  $\lambda = 10$ ,  $D = 38$ , and  $\Omega = 0.9$  at time, (a)  $t = 0$  and (b)  $t = 800$ .

the vortices are arranged in a hexagonal lattice as shown in Fig. 5(b). At  $\Omega = 0.8$  the vortex structure is shown in Fig. 5(c) resembles the structures observed in the references [18, 22] for dipolar condensates. In further, we observed the square lattice at  $\Omega = 0.9$ . To test the stability of the vortex structures, the ground state is evolved in real-time for the same parameters of imaginary time. The vortex structure persisted as depicted in Fig. 6, even after such long evolution of time.

At high rotation frequency (eg.  $\Omega = 0.995$ ) we found 16 vortices as shown in Fig. 7(f). Moreover, one may note from Fig. 4 that, for obtaining the vortex states in the condensates with larger dipolar strength, it is necessary to consider significantly large pan-cake trap. In this case we choose the trap aspect ratio  $\lambda = 30$  with dipolar interaction strength  $D \simeq 300$  corresponding to about 118000  $^{52}\text{Cr}$  atoms. We observed a similar arrangement in the vortex structures in  $\lambda = 10$  and 30, when the the number of vortices are equal. It tells us that the condensate tries to persist with the similar vortex structures even though the trap aspect ratio or dipolar interaction strength are distinct. For instance, we noticed a qualitatively similar array of vortex lattices for both  $\lambda = 10$  (see Fig. 6) and  $\lambda = 30$  (see Fig. 7(b)), with  $\Omega = 0.9$  and 0.3, respectively. Also we witnessed qualitatively similar structures for  $\lambda = 10$  (see Fig. 5(d)) and  $\lambda = 30$  (see Fig. 7(c)), with  $\Omega = 0.97$  and 0.4, respectively. The condensate in a strong pancake trap creates large number of vortices even at low rotation frequency.

Further, we observed some distortion in the vortex lattice structure when the number of vortices are larger. In particular the distortion is large near to the surface than the center of the condensate. All the vortices have the same charge of vorticity and their repulsion keeps the stable configuration. We also note that the size of the vortex core radius becomes significantly larger in the vicinity of the surface than in the middle of the condensate while increasing the rotation frequency. Consequently, near to surface repulsive interaction makes less density of vor-

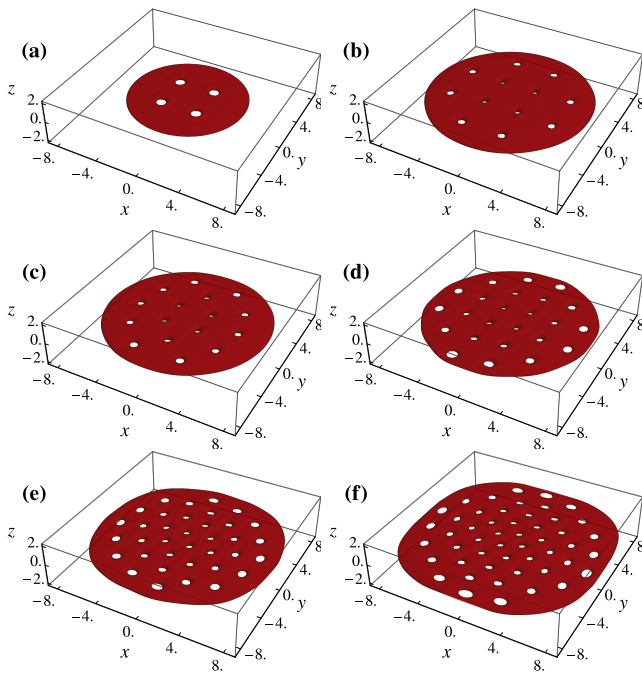


FIG. 7. (Color online) Three-dimensional view of condensate density  $|\phi(x, y, z)|^2$  with vortex lattice of purely dipolar BECs with  $a_{dd} = 16 a_0$ ,  $a = 0$ ,  $D = 300$ ,  $\lambda = 30$  at rotation frequencies (a)  $\Omega = 0.27$ ,  $|\phi(x, y, z)|^2 = 0.0125$ , (b)  $\Omega = 0.3$ ,  $|\phi(x, y, z)|^2 = 0.005$ , (c)  $\Omega = 0.4$ ,  $|\phi(x, y, z)|^2 = 0.005$  and (d)  $\Omega = 0.5$ ,  $|\phi(x, y, z)|^2 = 0.005$  (e)  $\Omega = 0.8$ ,  $|\phi(x, y, z)|^2 = 0.005$ , and (f)  $\Omega = 0.97$ ,  $|\phi(x, y, z)|^2 = 0.004$ .

tices and leads to the distortion in the vortex lattice. It is equivalent to observing transverse shear waves in quantum gases for the larger rotation frequencies [5]. In this regime there will be a decrease in the elastic shear strength of lattice takes place.

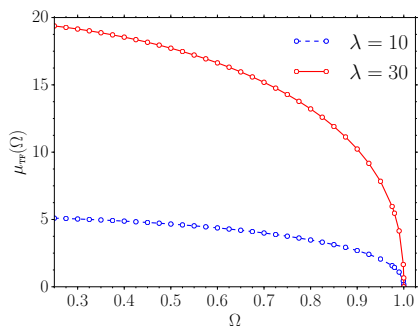


FIG. 8. (color online) Plot of the chemical potential as a function of the rotation frequency  $\Omega$  for the dipolar BEC trapped in  $\lambda = 10$  with  $D \simeq 38$  and  $\lambda = 30$  with  $D \simeq 300$ . In the both cases, the scattering length  $a = 1a_0$ .

Next, we calculate some physical quantities such as chemical potential, radius and angular momentum as a function of rotation frequency for trap aspect ratios

$\lambda = 10$  and  $30$  and are shown in Figs 8, 9 and 10. First, we calculate the chemical potential with respect to rotation frequency in mean-field Thomas-Fermi (TF) regime. When the interaction energy is large compared to the kinetic energy, the kinetic energy can be neglected and enters into TF regime. We assume the normalized density of the dipolar BEC of the form [34–37]

$$n(\mathbf{r}, t) \equiv |\phi(\mathbf{r}, t)|^2 = \frac{15}{8\pi R_\rho^2(t) R_z(t)} \left[ 1 - \frac{\rho^2}{R_\rho^2(t)} - \frac{z^2}{R_z^2(t)} \right], \quad (5)$$

where  $R_\rho(t)$  and  $R_z(t)$  are the radial and axial sizes. In the TF regime one has the following set of coupled ordinary differential equations for the evolution of the condensate sizes [35]:

$$\ddot{R}_\rho = \frac{15aN}{R_\rho R_z} \left[ \frac{1}{R_\rho^2} - \epsilon_{dd} \left( \frac{1}{R_\rho^2} + \frac{3}{2} \frac{f(\bar{\kappa})}{R_\rho^2 - R_z^2} \right) \right] - R_\rho \gamma^2, \quad (6)$$

$$\ddot{R}_z = \frac{15aN}{R_\rho^2} \left[ \frac{1}{R_z^2} + 2\epsilon_{dd} \left( \frac{1}{R_z^2} + \frac{3}{2} \frac{f(\bar{\kappa})}{R_\rho^2 - R_z^2} \right) \right] - \lambda^2 R_z. \quad (7)$$

with  $\kappa = R_\rho/R_z$ ,  $\epsilon_{dd} = a_{dd}/a$  and

$$f(\kappa) = \frac{1 + 2\kappa^2 - 3\kappa^2 d(\kappa)}{1 - \kappa^2}, \quad d(\kappa) = \frac{a \tanh \sqrt{1 - \kappa^2}}{\sqrt{1 - \kappa^2}}. \quad (8)$$

The dimensionless ratio  $\epsilon_{dd}$  connects the atomic scattering length and DDI. Here the atomic scattering length is taken as  $a = 1a_0$  in order to force the dominant dipolar effect. It may be noted that the external rotation expands the condensate radially and shrinks it axially. As a consequence, the dependence of TF radii on  $\Omega$  can be given by [6],

$$\frac{R_\rho(\Omega)}{R_\rho(0)} = (1 - \Omega^2)^{-3/10}, \quad \frac{R_z(\Omega)}{R_z(0)} = (1 - \Omega^2)^{1/5}. \quad (9)$$

Also, the chemical potential has the form,

$$\mu_{TF}(\Omega) = \mu_{TF}(0) (1 - \Omega^2)^{2/5}. \quad (10)$$

The chemical potential decreases continuously with increase in rotation frequency. As shown in Fig. 8 the chemical potential decreases continuously and it falls down to zero when  $\Omega = 1.0$ . In Fig. 9 we plot the rms radius and chemical potential as a function of rotation frequency calculated from the numerical solution of GP equation. As expected, the condensate radius increases with the increase of rotation frequency due to the expansion of condensate. The rms radius is shown in Figs. 9(a) and (b) for  $\lambda = 10$  and  $30$ , respectively. One may note that, in the absence of rotation, the numerically calculated chemical potential compares well with TF results [33]. Whereas, in the presence of rotation, the TF chemical potential is about two times less than the numerically calculated value. In Figs. 9(c) and (d) we show

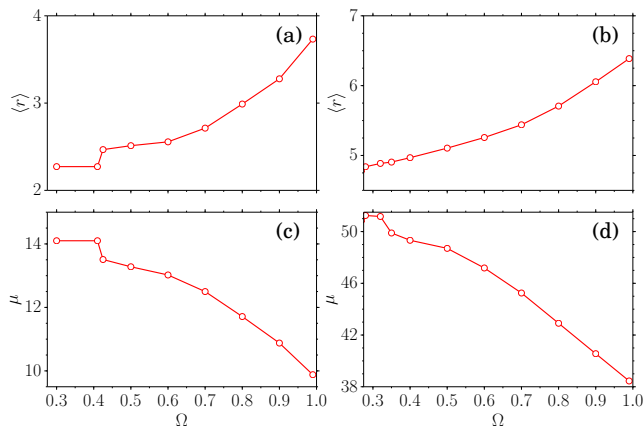


FIG. 9. Plot of the chemical potential and radius as a function of the rotation frequency  $\Omega$  for the purely dipolar BEC trapped in  $\lambda = 10$  in (a), (b) and 30 in (c), (d).

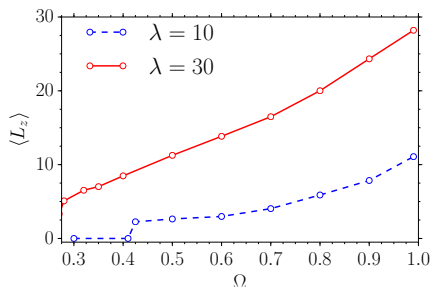


FIG. 10. (color online) Plot of the expectation value of angular momentum  $\langle L_z \rangle$  as a function of the rotation frequency  $\Omega$  for the purely dipolar BEC trapped in  $\lambda = 10$  and 30.

the variation of chemical potential for  $\lambda = 10$  and 30, respectively. Next, we calculate expectation value of angular momentum as a function of  $\Omega$  from the numerical solution. Fig. 10 depicts the plot of  $\langle L_z \rangle$  with respect to  $\Omega$  for  $\lambda = 10$  and 30. The increase in the  $\langle L_z \rangle$  is associated with the entry of vortices into the condensate. We are also interested to study the dependence of the vortex number ( $N_v$ ) on the rotational frequency  $\Omega$  in purely dipolar BEC. The rotating condensate has a dense array of vortices with a uniform density  $n_v = m(\Omega\bar{\omega})/\pi\hbar$ . The number of vortices present in the condensate is [6],

$$N_v = \frac{m(\Omega\bar{\omega})}{\hbar} R_\rho^2(\Omega). \quad (11)$$

The number of vortices increases linearly with  $\Omega$  assuming the BEC in a fixed axially symmetric harmonic trap. The radius  $R_\rho(0)$  in TF regime can be calculated from Eq. (7) and corresponding  $R_\rho(\Omega)$  can be obtained from Eq. (9). We have estimated the number of vortices in the different harmonic trap aspect ratios  $\lambda = 10, 20$  and 30 in TF regime and compared with numerically calculated equilibrium numbers, and plotted the results in

Fig. 11(a). We noted some deviations in the number of vortices from TF results and calculated numerically. To compare the deviation in the number of vortices in BEC without DDI, we continued the calculation of  $N_v$  for the BEC without DDI by tuning  $\varphi = 54.7^\circ$  to magic angle where the dipolar interaction averages to zero in Eq. (4). Then we calculated  $N_v$  at  $a = 50a_0$  and  $100a_0$  and we observed the deviation as shown in Fig. 11(b). In partic-

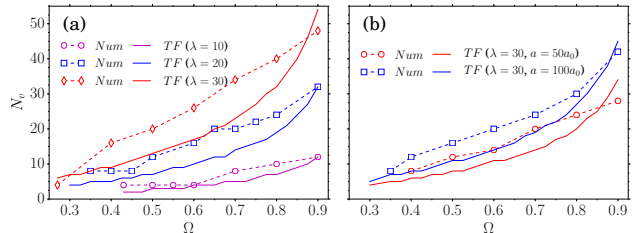


FIG. 11. (color online) Plot of the equilibrium vortex number ( $N_v$ ) as a function of the rotation frequency  $\Omega$  for the (a) purely dipolar BEC trapped in  $\lambda = 10, 20$  and 30, and (b) non-dipolar BEC trapped in  $\lambda = 30$ .

ular, when  $\Omega > 0.9$  the deviation is larger and it is due to the strong expansion of condensate during the rapid rotation.

## V. VORTEX LATTICE IN FULLY ANISOTROPIC TRAP

Finally, we concerned the purely dipolar BEC trapped in fully anisotropic trap with  $\gamma \neq \nu \neq \lambda$  in the Eq. (3). Whenever  $\gamma \neq \nu$ , the system breaks the cylindrical symmetry. For the present analysis, we shall fix  $\lambda = 10$ ,  $\nu = 1$ , and vary  $\gamma$  to study the changes in the spatial distribution of vortices in purely dipolar BECs by increasing eccentricity of the trapping potential along  $x$ -direction. The condensate strongly elongates along the  $x$ -direction

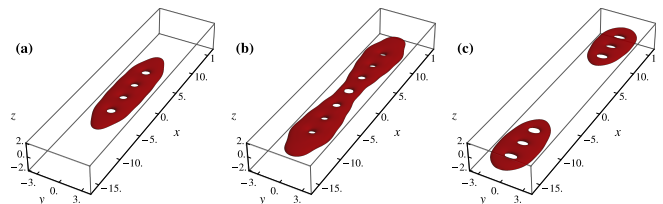


FIG. 12. (Color online) Vortex lattices of condensate ground state in rotating dipolar BECs trapped in asymmetric trap with  $\gamma = 0.5$ ,  $\lambda = 10$ ,  $D = 38$  and rotation frequency: (a)  $\Omega = 0.425$ , (b)  $\Omega = 0.6$ , (c)  $\Omega = 0.7$ . The contour levels are taken at  $|\phi(x, y, z)|^2 = 0.01, 0.005$  and  $0.01$ , respectively.

at  $\gamma \leq 0.5$ . The rotational force also elongates the condensate along  $x$ -direction. We have shown four linearly arranged vortices in Fig. 12(a) for  $\gamma = 0.5$  and  $\Omega = 0.425$ .

In addition to the repulsive dipolar force between condensate atoms the rotation provides supplementary elongation. Consequently, the centrifugal force due to rotation splits the condensate into two parts along the weakly trapped  $x$ -direction when  $\Omega = 0.7$  as shown in Fig. 12(c). After this splitting, the number and arrangements of vortices are similar in each part. We have observed only two vortices as shown in Fig. 13(a) at  $\gamma = 0.7$  for the rotation frequency  $\Omega = 0.425$ . This is exactly half the number of

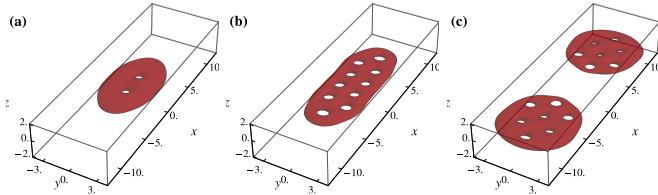


FIG. 13. (Color online) Vortex lattices of condensate ground state in rotating dipolar BECs trapped in asymmetric trap with  $\gamma = 0.7$ ,  $\lambda = 10$ ,  $D = 38$  and rotation frequency: (a)  $\Omega = 0.425$ , (b)  $\Omega = 0.7$ , (c)  $\Omega = 0.91$ . The contour levels are taken at  $|\phi(x, y, z)|^2 = 0.01$ ,  $0.01$  and  $0.005$ , respectively.

vortices when compared to that with  $\gamma = 0.5$  for the same rotation frequency. This evidences the dependence of number of vortices on the strength of eccentricity of the trap. We have also witnessed the zig-zag arrangement of vortices for  $\gamma > 0.5$  as shown in Fig. (13)(b). Besides the strong rotation the condensate splits into two parts. Here the splitting at  $\Omega = 0.91$  indicates that stronger condensate with large  $\gamma$  requires substantially larger rotation frequency than the condensate with less  $\gamma$ . We calculated the critical rotation frequency ( $\Omega_{sp}$ ) for splitting of the condensate with respect to the eccentricity of the trap  $\gamma$  and shown in Fig. (14).

We have observed the linear and zig-zag arrangement of vortices with respect to the strength of eccentricity of the trap in the Figs. 12 and 13, respectively. Such kind of linear and zigzag vortex configuration has been observed in normal BEC with two-dimensional model [38].

## VI. SUMMARY AND CONCLUSION

In summary, we have studied the ground state vortex lattice structures of purely dipolar Bose-Einstein condensate of  $^{52}\text{Cr}$  atoms by considering the full three dimensional Gross-Pitaevskii equation. We have identified the stability regimes for ground as well as vortex state in purely dipolar BECs with respect to both trap aspect ratio and dipole-dipole interaction strength. The stability of vortex lattice structures has been confirmed by real time evolution. We have shown stationary vortex

lattice structures for different trap aspect ratios within the stability regime. Also distortions in the lattices at high rotation frequencies has been observed. We have witnessed similar arrangement of vortex structures for

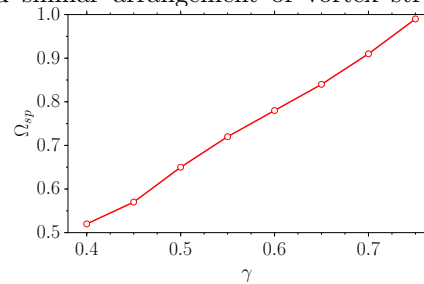


FIG. 14. Critical rotation frequency for the separation of condensate during rotation with respect to anisotropy of the trap along  $x$ -direction.

different trap aspect ratios provided the number of vortices are equal. The number of vortices has been calculated using Thomas-Fermi approximation and they were compared with that obtained through numerical simulations. Further, we have analysed the spatial distribution of vortices in fully anisotropic trap and observed linear and zig-zag arrangement of vortices. Also we noticed breaking up of the condensates into two parts with equal number of vortices due to strong dipolar strength and high rotation frequency.

The predicted phase diagram for the stable vortex state will be useful to demonstrate the parameters such as dipolar strengths and trap aspect ratios for making experimental and theoretical studies on rotating dipolar quantum gases. In further, the stability regime is of wider interest to investigate rapidly rotating dipolar BECs in the lowest Landau level. The dipolar BECs has unique vortex states like hexagonal and square vortex lattices due to the presence of the dipolar interaction. Breaking in the rotating dipolar BECs in fully anisotropic trap will be a fascinating experimental exploration.

## ACKNOWLEDGMENTS

RKK acknowledges the financial support from FAPESP of Brazil (Contract number 2014/01668-8). TS acknowledges financial support from University Grants Commission, India in the form UGC-RFSMS fellowship. The work of PM forms a part of Science & Engineering Research Board, Department of Science & Technology, Govt. of India sponsored research project (SERB Ref. No. EMR/2014/000644). AG and HF acknowledges CAPES, CNPq and FAPESP of Brazil.

[1] M. R. Matthews, B. P. Anderson, P. C. Haljan, D. S. Hall, C. E. Wieman, and E. A. Cornell, Vortices in a Bose-

Einstein condensate, Phys. Rev. Lett. **83**, 2498 (1999).

- [2] K. W. Madison, F. Chevy, W. Wohlleben, and J. Dalibard, Vortex formation in a stirred Bose-Einstein condensate, *Phys. Rev. Lett.* **84**, 806 (2000); J. R. Abo-Shaeer, C. Raman, J. M. Vogels, and W. Ketterle, Observation of vortex lattices in Bose-Einstein condensates, *Science* **292**, 476-479 (2001); V. Schweikhard, S. Tung, and E. A. Cornell, Vortex proliferation in the Berezinskii-Kosterlitz-Thouless regime on a two-dimensional lattice of Bose-Einstein condensates, *Phys. Rev. Lett.* **99** 030401 (2007); R. A. Williams, S. Al-Assam, and C. J. Foot, Observation of vortex nucleation in a rotating two-dimensional lattice of Bose-Einstein condensates, *Phys. Rev. Lett.* **104**, 050404 (2010).
- [3] K. P. Marzlin and W. Zhang, Quantized circular motion of a trapped Bose-Einstein condensate: Coherent rotation and vortices, *Phys. Rev. A* **57**, 4761 (1998); L. Salasnich, A. Parola, and L. Reatto, Bosons in a toroidal trap: Ground state and vortices, *Phys. Rev. A* **59**, 2990 (1999); I. Danaila, Three-dimensional vortex structure of a fast rotating Bose-Einstein condensate with harmonic-plus-quartic confinement, *Phys. Rev. A* **72**, 013605 (2005); K. Kasamatsu, M. Machida, N. Sasa, and M. Tsubota, Three-dimensional dynamics of vortex-lattice formation in Bose-Einstein condensates, *Phys. Rev. A* **71**, 063616 (2005); T. P. Simula and K. Machida, Kelvin-Tkachenko waves of few-vortex arrays in trapped Bose-Einstein condensates, *Phys. Rev. A* **82**, 063627 (2010); W. Bao, D. Marahrens, Q. Tang, and Y. Zhang, A simple and efficient numerical method for computing the dynamics of rotating Bose-Einstein condensates via rotating Lagrangian coordinates, *J. Sci. Comput.* **35**(6), A2671-A2695 (2013); D. S. Dantas D, A. R. P. Lima, A. Chaves, C. A. S. Almeida, G. A. Farias, and M. V. Milošević, Bound vortex states and exotic lattices in multicomponent Bose-Einstein condensates: The role of vortex-vortex interaction, *Phys. Rev. A* **91**, 023630 (2015).
- [4] J. J. Garcia-Ripoll and V. M. Pérez-García, Vortex bending and tightly packed vortex lattices in Bose-Einstein condensates, *Phys. Rev. A* **64**, 053611 (2001); A. Aftalion and I. Danaila, Three-dimensional vortex configurations in a rotating Bose-Einstein condensate, *Phys. Rev. A* **68**, 023603 (2003).
- [5] I. Coddington, P. Engels, V. Schweikhard, and E. A. Cornell, Observation of Tkachenko oscillations in rapidly rotating Bose-Einstein Condensates, *Phys. Rev. Lett.* **91**, 100402 (2003).
- [6] A. Fetter, Rotating trapped Bose-Einstein condensates, *Rev. Mod. Phys.* **81**, 647 (2009); P. G. Kevrekidis, R. Carretero-González, D. J. Frantzeskakis, and I. G. Kevrekidis, Vortices in Bose-Einstein condensates: Some recent developments, *Mod. Phys. Lett. B* **18**, 1481 (2004); A. L. Fetter and A. A. Svidzinsky, Vortices in a trapped dilute Bose-Einstein condensate, *J. Phys. : Condens. Matter* **13**, R135 (2001).
- [7] A. Minguzzi, S. Succi, F. Toschi, M. P. Tosi and P. Vignolo, Numerical methods for atomic quantum gases with applications to Bose-Einstein condensates and to ultracold fermions, *Phys. Rep.* **395**, 223 (2004).
- [8] K. W. Madison, F. Chevy, W. Wohlleben, and J. Dalibard, Vortex Formation in a stirred Bose-Einstein condensate, *Phys. Rev. Lett.* **84**, 806 (2000); B. P. Anderson, P. C. Haljan, C. A. Regal, D. L. Feder, L. A. Collins, C. W. Clark, and E. A. Cornell, Watching dark solitons decay into vortex rings in a Bose-Einstein condensate, *Phys. Rev. Lett.* **86** 2926 (2001); A. E. Leanhardt, A. Görlitz, A. P. Chikkatur, D. Kielpinski, Y. Shin, D. E. Pritchard, and W. Ketterle, Imprinting vortices in a Bose-Einstein condensate using topological phases, *Phys. Rev. Lett.* **89**, 190403 (2002); E. A. L. Henn, J. A. Seman, G. Roati, K. M. F. Magalhães, and V. S. Bagnato, Emergence of turbulence in an oscillating Bose-Einstein condensate, *Phys. Rev. Lett.* **103**, 045301 (2009).
- [9] J. Dalibard, F. Gerbier, G. Juzeliūnas, and P. Öhberg, Colloquium: Artificial gauge potentials for neutral atoms, *Rev. Mod. Phys.* **83**, 1523 (2011).
- [10] A. Aftalion and Q. Du, Vortices in a rotating Bose-Einstein condensate: Critical angular velocities and energy diagrams in the Thomas-Fermi regime, *Phys. Rev. A* **64**, 063603(R) (2001); L. O. Baksmaty, Y. Liu, U. Landman, N. P. Bigelow, and H. Pu, Numerical exploration of vortex matter in Bose-Einstein condensates, *Math. Comput. Simulat.* **80**, 131 (2009); B. W. Jeng, Y. S. Wang, and C. S. Chien, A two-parameter continuation algorithm for vortex pinning in rotating Bose-Einstein condensates, *Comp. Phys. Commun.* **184**, 493 (2013).
- [11] A. Griesmaier, J. Werner, S. Hensler, J. Stuhler, and T. Pfau, Bose-Einstein condensation of Chromium, *Phys. Rev. Lett.* **94**, 160401 (2005).
- [12] M. Lu, N. Q. Burdick, S. H. Youn, and B. L. Lev, Strongly dipolar Bose-Einstein condensate of Dysprosium, *Phys. Rev. Lett.* **107**, 190401 (2011).
- [13] K. Aikawa, A. Frisch, M. Mark, S. Baier, A. Rietzler, R. Grimm, and F. Ferlaino, Bose-Einstein condensation of Erbium, *Phys. Rev. Lett.* **108**, 210401 (2012).
- [14] M. A. Baranov, Theoretical progress in many-body physics with ultracold dipolar gases, *Phys. Rep.* **464**, 71-111 (2008).
- [15] J. Lahaye, C. Menotti, L. Santos, M. Lewenstein, and T. Pfau, The physics of dipolar bosonic quantum gases, *Rep. Prog. Phys.* **72**, 126401 (2009).
- [16] L. E. Young-S and S. K. Adhikari, Mixing, demixing, and structure formation in a binary dipolar Bose-Einstein condensate, *Phys. Rev. A* **86**, 063611 (2012); Dipolar droplet bound in a trapped Bose-Einstein condensate, *Phys. Rev. A* **87**, 013618 (2013).
- [17] P. A. Andreev and L. S. Kuz'menkov, Dispersion properties of transverse waves in electrically polarized BECs, *J. Phys. B* **47**, 225301 (2014).
- [18] S. Yi and H. Pu, Vortex structures in dipolar condensates, *Phys. Rev. A* **73**, 061602(R) (2006).
- [19] R. M. Wilson, S. Ronen and J. L. Bohn, Stability and excitations of a dipolar Bose-Einstein condensate with a vortex, *Phys. Rev. A* **79**, 013621 (2009).
- [20] M. Abad, M. Guilleumas, R. Mayol, M. Pi, and D. M. Jezek, Vortices in Bose-Einstein condensates with dominant dipolar interactions, *Phys. Rev. A* **79**, 063622 (2009); Dipolar condensates confined in a toroidal trap: Ground state and vortices, *Phys. Rev. A* **81**, 043619 (2010).
- [21] R. M. W. van Bijnen, D. H. J. O'Dell, N. G. Parker, and A. M. Martin, Dynamical instability of a rotating dipolar Bose-Einstein condensate, *Phys. Rev. Lett.* **98**, 150401 (2007); R. M. W. van Bijnen, A. J. Dow, D. H. J. O'Dell, N. G. Parker, and A. M. Martin, Exact solutions and stability of rotating dipolar Bose-Einstein condensates in the Thomas-Fermi limit, *Phys. Rev. A* **80**, 033617 (2009).



- [22] F. Malet, T. Kristensen, S. M. Reimann, and G. M. Kavoulakis, Rotational properties of dipolar Bose-Einstein condensates confined in anisotropic harmonic potentials, *Phys. Rev. A* **83**, 033628 (2011).
- [23] R. K. Kumar and P. Muruganandam, Vortex dynamics of rotating dipolar Bose-Einstein condensates, *J. Phys. B* **45**, 215301 (2012).
- [24] R. K. Kumar and P. Muruganandam, Effect of optical lattice potentials on the vortices in rotating dipolar Bose-Einstein condensates, *Eur. Phys. J. D* **68**, 289 (2014).
- [25] S. Ronen, D. C. E. Bortolotti, and J. L. Bohn, Radial and angular rotons in trapped dipolar gases, *Phys. Rev. Lett.* **98**, 030406 (2007).
- [26] O. Dutta and P. Meystre, Ground-state structure and stability of dipolar condensates in anisotropic traps, *Phys. Rev. A* **75**, 053604 (2007); A. D. Martin and B. P. Blakie, Stability and structure of an anisotropically trapped dipolar Bose-Einstein condensate: Angular and linear rotons, *Phys. Rev. A* **86**, 053623 (2012).
- [27] W. Bao and H. Wang, An efficient and spectrally accurate numerical method for computing dynamics of rotating Bose-Einstein condensates, *J. Comput. Phys.* **217**, 612 (2006).
- [28] S. Giovanazzi, A. Görlitz, and T. Pfau, Tuning the dipolar interaction in quantum gases, *Phys. Rev. Lett.* **89**, 130401 (2002).
- [29] K. Góral and L. Santos, Ground state and elementary excitations of single and binary Bose-Einstein condensates of trapped dipolar gases, *Phys. Rev. A* **66**, 023613 (2002).
- [30] T. Koch, T. Lahaye, Fröhlich, A. Griesmaier, and T. Pfau, Stabilization of a purely dipolar quantum gas against collapse, *Nature Phys.* **4**, 218-222 (2008).
- [31] M. Brtko, A. Gammal, and L. Tomio, Relaxation algorithm to hyperbolic states in Gross-Pitaevskii equation, *Phys. Lett. A* **359**, 339 (2006).
- [32] P. Muruganandam and S. K. Adhikari, Fortran programs for the time-dependent Gross-Pitaevskii equation in a fully anisotropic trap, *Comput. Phys. Commun.* **180**, 1888-1912 (2009).
- [33] R. K. Kumar, L. E. Young-S, D. Vudragović, A. Balaž, P. Muruganandam, and S. K. Adhikari, Fortran and C programs for the time-dependent dipolar Gross-Pitaevskii equation in an anisotropic trap. *Comput. Phys. Commun.* **195**, 117-128 (2015).
- [34] F. Dalfovo, S. Giorgini, L. P. Pitaevskii, and S. Stringari, Theory of Bose-Einstein condensation in trapped gases, *Rev. Mod. Phys.* **71**, 463-512 (1999).
- [35] D. H. J. O'Dell, S. Giovanazzi, and C. Eberlein, Exact hydrodynamics of a trapped dipolar Bose-Einstein condensate, *Phys. Rev. Lett.* **92**, 250401 (2004).
- [36] C. Eberlein, S. Giovanazzi, and D. H. J. O'Dell, Exact solution of the Thomas-Fermi equation for a trapped Bose-Einstein condensate with dipole-dipole interactions, *Phys. Rev. A* **71**, 033618 (2005).
- [37] N. G. Parker and D. H. J. O'Dell, Thomas-Fermi versus one- and two-dimensional regimes of a trapped dipolar Bose-Einstein condensate, *Phys. Rev. A* **78**, 041601(R) (2008).
- [38] N. L. Gullo, T. Busch, and M. Paternostro, Structural change of vortex patterns in anisotropic Bose-Einstein condensates, *Phys. Rev. A* **83**, 053612 (2011).